Contents lists available at ScienceDirect

Applied Catalysis B: Environmental

Porous N,P-doped carbon from coconut shells with high electrocatalytic activity for oxygen reduction: Alternative to Pt-C for alkaline fuel cells

Maryam Borghei [a],[*], Nikorn Laocharoen [a], Elo Kibena-Põldsepp [b], Leena-Sisko Johansson [a], Joseph Campbell [a], Esko Kauppinen [c], Kaido Tammeveski [b], Orlando J. Rojas [a],[c],[*]

[a] Bio-Based Colloids and Materials, and Centre of Excellence on "Molecular Engineering of Biosynthetic Hybrid Materials Research" (HYBER), Department of Bioproducts & Biosystems, Aalto University, Finland
[b] Institute of Chemistry, University of Tartu, Estonia
[c] Nanomaterials Group, Department of Applied Physics, Aalto University, Finland

ABSTRACT

This study introduces a new, environmentally-friendly method to synthesize N,P-doped porous carbon by high conversion (46% yield) of coconut shell residues for the reduction of oxygen in alkaline media. The obtained materials display an excellent electrocatalytic activity, making them suitable as cathode catalyst for alkaline fuel cells. The synthesis procedure included an efficient single-step activation with phosphoric acid to achieve high surface area ($1216\,m^2\,g^{-1}$) and pore volume ($1.15\,cm^3\,g^{-1}$ with 72% mesopores). Urea was used as a low-cost and ecologically-sound source for nitrogen doping of the as-synthesized porous carbon. Remarkably, the biomass-derived electroactive carbon demonstrates a superior performance compared to a reference material, the state-of-the-art commercial Pt-C catalyst: (a) comparable electrocatalytic activity; (b) better tolerance to methanol crossover effects and, (c) improved long-term durability towards oxygen reduction reaction in alkaline media.

© 2016 Elsevier B.V. All rights reserved.

1. Introduction

Fuel cells are promising and sustainable energy conversion alternatives owing to associated null or low greenhouse gas emission and high efficiency (~80%). However, the large scale application of fuel cells is limited by the need of incorporating expensive Pt-based catalysts in their cathodic and anodic electrode components [1,2]. Therefore, low-platinum or metal-free electrocatalysts are most desirable for fuel cells to enter the market [3]. Recently, nitrogen doping of carbon nanotubes (CNT) and graphene were reported to be beneficial to enhance the oxygen reduction reaction (ORR) in alkaline conditions [4]. Nitrogen doping effectively modulates the surface chemistry, electron-donor ability and electrochemical properties of the sp^2 carbon structure, as it has been confirmed by experiments and density functional theory (DFT) calculations [5–8]. In addition, compared to single-atom doping, co-doping with other heteroatoms such as S, P and B improves the electrocatalytic activity for the ORR [9,10].

Despite the outstanding properties of graphene and CNT, they are still expensive and their synthesis in large scale inherently involves the use of natural gas or hazardous chemicals as well as metals as catalyst precursors [11]. Lignocellulosic biomass in the form of plant materials as well as wastes from household and animal husbandry is an abundant and renewable alternative for conversion to novel value-added carbon products. Their use can additionally address issues related to waste disposal and accumulation. According to the United Nations, almost 140 billion metric tons of biomass is generated globally from agricultural waste [12]. Therefore, converting biomass can potentially reduce the use of fossil fuels as well as greenhouse gas release, while closing the carbon cycle loop and promoting economic incentives [13].

Nowadays, increasing attention is given towards porous carbons with electroactive properties produced from natural resources and lignocellulosic biomass. N-doped carbon materials have been synthesized for example from bacterial cellulose [14,15], cellulose

* Corresponding authors at: Bio-Based Colloids and Materials, and Centre of Excellence on "Molecular Engineering of Biosynthetic Hybrid Materials Research" (HYBER), Department of Bioproducts & Biosystems, Aalto University, Finland.
E-mail addresses: maryam.borghei@aalto.fi, mary.borghei@gmail.com (M. Borghei), Orlando.rojas@aalto.fi (O.J. Rojas).

nanocrystals [16], glucose and soy proteins [17], chitin [18,19], chitosan [20–22], lignin [23], and plant biomass (*Eichhornia cras-sipes* [24], and *Typha orientalis* [25]). In addition, heteroatom-doped carbons have been explored, for example, via pyrolysis of cellulose phosphate to yield P-doped carbon [26]; N,P-doped carbon from cellulose nanocrystals and ammonium phosphate [27]; N,S-doped carbon from human hair [28] or glucose and those derived from S-containing precursors such as S-(2-Thienyl)-ʟ-cysteine, 2-Thienyl-carboxaldehyde, ʟ-cysteine [29,30]. The synthesis of multiple heteroatom-doped carbon has also been reported by direct pyrolysis of ginkgo leaves [31] and seaweeds [32].

Among abundant bioresoures, coconut shells represent an important residue in tropical areas, available in large quantities. Additionally, they display high carbon content and low ash residues (<1 wt.%) [33,34]. Owing to their large lignin content (~30–49 wt.%), the elemental composition of coconut shells includes high carbon (~53–64 wt.%) and low H/C and O/C ratios [35–37]. Moreover, compared to other agricultural biomass, the density of the raw coconut shells is one of the highest (1.31) while their porosity is among the lowest (14.9%) [37]. This stems from the strong cross-linking of cellulose, hemicelluloses and lignin components in the plant cells. Therefore, the coconut shells are expected to be well suited as source material for the production of activated carbon with high adsorption capacity, bulk density and hardness. Recently, Yang et al. synthesized N-doped porous carbon for CO_2 adsorption with a micropore-dominant structure [38]. Despite the high adsorption capacity, the synthesis process involved multiple steps, such as separate carbonization and activation along with ammoxidation treatment (ammonia/air) for nitrogen doping. Zhao et al. suggested catalytic production of vinyl chloride on N-doped activated carbon by using melamine as N-containing precursor [39]. In contrast, the present work is designed to obtain an electroactive N,P-doped mesoporous carbon via an economical and environmentally-sound process through a single-step activation with phosphoric acid, followed by nitrogen doping using urea. In turn, this valorization of biomass for development of novel catalytic materials addresses the need for reducing hazardous chemicals.

There are two main methods for the activation of lignocellulosic materials; either by physical or chemical processes [35]. Physical activation is carried out in two separate steps: a preliminary carbonization in an inert atmosphere at intermediate temperatures (400–500 °C), followed by activation using steam or carbon dioxide at higher temperatures (900–1000 °C) [40]. Chemical activation is done via impregnation of the raw material with given chemicals at specific proportions before carbonization. Potassium hydroxide (KOH), sodium hydroxide (NaOH), sodium carbonate (Na_2CO_3), magnesium chloride ($MgCl_2$), phosphoric acid (H_3PO_4) and zinc chloride ($ZnCl_2$) have been reported as typical dehydrating agents for chemical activation [41–43]. Phosphoric acid is an ideal reagent due to its low-cost, low environmental impact, milder than zinc chloride, and produces high surface area carbon with desired pore size distribution, in a single-step and at low temperatures (400–500 °C) [44]. Furthermore, chemical activation of coconut shells with phosphoric acid can generate crack-free active carbon grains, leading to the better mechanical properties compared to those of carbon activated via $ZnCl_2$ [35]. Urea is a non-toxic, inexpensive and environmentally safe alternative among precursors of graphitic carbon nitride (g-C_3N_4) such as thiourea, dicyandiamide and melamine [45]. Besides, urea presents a higher water solubility and can result in denser C–N sp^2 graphitic structures at 500 °C [46]. This study shows for the first time the development of N,P-doped porous carbons derived from coconut shells with high electrocatalytic activity towards the reduction of oxygen in alkaline media.

2. Experimental

2.1. Material synthesis

The carbon samples were prepared after chemical activation of coconut shells with phosphoric acid, followed by doping with urea as nitrogen precursor and pyrolysis at 1000 °C. In more detail, coconuts were purchased from a local market (S-Market, Finland) and their shells were grinded and sieved through 100 μm mesh. The powdered materials were chemically impregnated overnight with 50 wt.% H_3PO_4 (1:2 ratio), followed by drying at 70 °C until a paste texture was obtained. The carbonization was carried out under nitrogen flow at 550 °C for 1 h using a heating ramp rate of 10 °C min^{-1}. The obtained carbon was washed with hot water and then immersed in 3 M HCl overnight and finally filtered and dried at 105 °C. For nitrogen doping of the activated carbon (AC), a post-treatment was performed by dispersion in 1 M urea solution overnight. The resultant dispersion was filtered and dried, followed by pyrolysis at 1000 °C for 2 h at 5 °C min^{-1}. In order to enhance the interaction of urea with the surface of the activated carbon, the AC was treated with 2 M HNO_3/1 M H_2SO_4 (1:1 v/v) at 120 °C for 2 h (functionalization treatment). Herein, the samples are coded as *AC* for activated carbon; *AC-P* for the AC after pyrolysis at 1000 °C; *AC-U-P* for the impregnated *AC* with urea followed by pyrolysis and, finally, *AC-F-U-P* for the *AC* after functionalization and urea impregnation and pyrolysis. A schematic illustration of the latter synthesis procedure, the *AC-F-U-P* sequence, is provided in Fig. 1.

2.2. Characterization

Scanning electron microscopy (SEM) studies were carried out with a field emission Zeiss Sigma VP at 2 kV N_2 adsorption-desorption measurements were performed at 77 K using a Micromeritics Tristar II equipped with an automated surface area and pore size analyzer. Prior to the measurements, the samples were left in a degas system (Micromeritics II, Flow Prep 060) at 120 °C for 2 h under N_2 flow. The Brunauer-Emmett-Teller (BET) method was used to determine the specific surface area, while Barrett-Joyner-Halenda (BJH) method and the DFT were applied to obtain the pore volume and pore size distributions. The total pore volume (V_T) was obtained from the adsorption value at relative pressure (p/p$_0$) of 0.99. X-ray photoelectron spectroscopy (XPS) was utilized for the surface chemical analysis of the prepared materials, using AXIS Ultra electron spectrometer (Kratos Analytical, UK) with monochromatic Al Kα irradiation (incident energy = 1486.6 eV) at 100 W and under neutralization. Both elemental wide spectra as well as high resolution regional spectra for carbon, oxygen and nitrogen were recorded. Thermal gravimetric analysis (TGA) was performed using a Perkin Elmer TGA7 system in a temperature range of 20–900 °C at a heating rate of 10 °C min^{-1} under air condition. Raman spectroscopy was carried out using a Horiba LabRAM HR spectrometer equipped with CCD camera and 633 nm laser beam.

2.3. Electrochemical measurements

Catalyst inks were prepared by dispersing 15 mg of the respective carbon (*AC, AC-P, AC-U-P, AC-F-U-P*) in 476 μl of ethanol and 24 μl of FAA3 anion exchange ionomer (solution of 12 wt.% FAA3 in N-methyl-2-pyrrolydone, supplied by Fuma-Tech). Glassy carbon electrodes, GCE, (0.196 cm^2) were polished and a drop of 2 μl ink was deposited carefully to cover the whole surface. The modified GCE was dried under air flow and then in an oven at 60 °C for 2 h. The half-cell electrochemical measurements were performed in a 3-electrode cell consisting the modified GCE as working electrode (WE), a Pt-rod as a counter electrode (CE) and a Ag/AgCl (3 M KCl) as
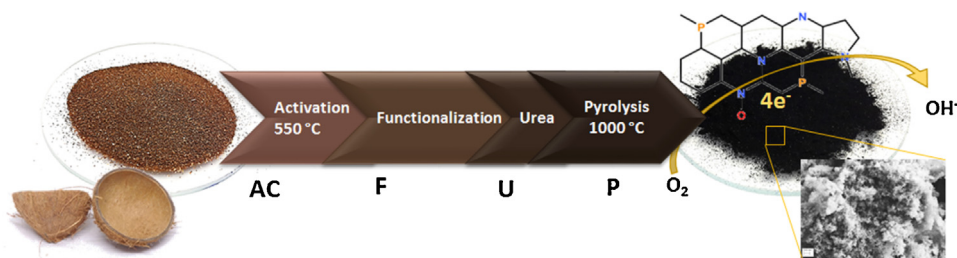
Fig. 1. Schematic of the synthesis of N,P-doped porous carbon from coconut shells (*AC-F-U-P*). Shorter sequences were also performed, for example, those with no functionalization *F* and/or no urea treatment *U* (*AC, AC-P, AC-U-P*).

reference electrode (RE), controlled by an Autolab PGSTAT12 potentiostat (Metrohm-Autolab, The Netherlands) and General Purpose Electrochemical System (GPES) software. The ORR measurements were carried out by cyclic voltammetry (CV) in an O_2-saturated 0.1 M KOH electrolyte in a potential range from 0.2 to −1.2 V at scan rate of 10 mV s^{-1}. Rotating disk electrode (RDE) measurements were performed at different rotation rates from 100 to 2500 rpm at 10 mV s^{-1}. The durability of the samples was also evaluated by chronoamperometric measurements at −0.3 V for almost 50,000 s (~13 h). The ORR activity and stability of the catalysts were compared with the state-of-the-art commercial catalyst consisting of 20 wt.% Pt supported on carbon black (Pt-C), purchased from Alfa Aesar.

3. Results and discussion

3.1. Physicochemical characterization and heteroatom doping

The surface morphology of the activated carbon indicates a highly porous, three-dimensional structure that was created upon chemical activation with phosphoric acid (SEM image in Fig. 2a). The N_2 adsorption isotherms and the pore distribution of *AC* and *AC-P* (Fig. 2b and c) confirmed the high porosity inferred from the SEM micrograph (Fig. 2a). A type IV isotherm with a hysteresis loop at relative pressure >0.4 indicated a dominant mesoporous structure. The low pressure region of the isotherm relates to the micropore filling, while the plateau at high relative pressures corresponds to the multilayer adsorption in the *meso-* and macropores. The specific surface area obtained for *AC* by the BET method was remarkable, 1216 m^2 g^{-1}, and the results included a large pore volume fraction (1.15 cm^3 g^{-1} with 72% of mesopores). The pore size distribution (Fig. 2c) showed a sharp peak at ~2 nm, followed by wide distribution of mesopores with 4.8 nm average pore size (Fig. 2d). The absence of isotherm plateau at high relative pressures together with the wide pore size distribution may indicate the presence of slit-like pores in an open structure [29].

In general, several parameters such as the source material, the activating chemicals and composition, carbonization temperature, time and the ramp rate influence significantly the surface area and the pore structure of the activated carbon [47]. The coconut shell was chosen in this study due to the high carbon content, low ash and sufficient hardness, which are beneficial for the final application as fuel cell electrocatalyst. This is due to the morphology of the coconut shell plant cell, which comprises tightly bound and cross-linked cellulose, hemicelluloses and lignin [37]. Furthermore, upon activation via phosphoric acid, the phosphate and phosphate ester form linkages to the lignocellulose, thereby inhibiting the shrinkage of the structure during the pyrolysis; as a result, the voids volume are protected [42]. Upon rinsing the sample after pyrolysis, the phosphate groups are washed away, forming large number of pores in the activated carbon structure. In addition, phosphoric acid retards the decomposition of ligno-

cellulose by preventing tar formation and the evolution of volatile products during the pyrolysis, thus providing high carbonization yield (TGA analysis in Fig. S1) [43]. Based on degradation temperature of impregnated coconut shells (see Fig. S1) and previous findings [48], the carbonization temperature was set at 550 °C to obtain high *AC* yield (46%). Such high carbon yield is a crucial factor in the cost of the final electrocatalyst for fuel cells. We also observed that by increasing the temperature ramp rate, higher number of mesopores were obtained (Fig. S2), which is desirable for the application in this study. Phosphoric acid, on one hand, works as hydrolyzing agent to cleave the lignocellulosic bonds and, on the other hand, acts as cross-linker via formation of phosphate ester linkages. Upon heat treatment of the lignocellulos-phosphoric acid mixture, crosslinking reactions initially dominate over bond cleavage, until ~250 °C. As the temperature is increased, cyclization and condensation occur due to the scission of P-O—C bonds. At faster heating ramps, the rate of phosphate bond cleavage occurs faster than the condensation and reordering of the clusters, leaving larger pores [49]. Therefore, a 10 °C min^{-1} heating rate was chosen to obtain wider mesopores contribution, with the additional benefit of decreasing the activation cost.

In the case of *AC-P*, heat-treatment of *AC* at 1000 °C (2 h) did not influence the pore structure. The BET surface area and pore volume of *AC-P* only decreased slightly, owing to carbon gasification. Interestingly, the N_2 adsorption isotherms and pore size distribution of *AC-U-P* and *AC-F-U-P* did not significantly change after further processing via acid functionalization (120 °C, 2 h) and urea impregnation (see Fig. S3). However, longer functionalization times, for 4 h, significantly damaged the pore structure (Fig. S4). Treatment with urea prevented gasification, possibly due to crosslinking and formation of graphitic carbon nitride sheets [50]. Notably, the pore structure and surface area of *AC-F-U-P* was still similar than those of the other samples (Fig. 2d), even after functionalization treatment. This indicated a high mechanical strength of the activated carbon produced from the coconut shells [51].

The XPS survey spectrum of the carbon samples (Fig. 3a) shows a strong carbon C1 s peak at 284.3 eV as well as signals for oxygen (O1 s at around 532 eV) and phosphorus (P2p at 133 eV and P2 s at 190.3 eV) [26,27]. According to the asymmetric shape of the sharp peak at 284.3 eV in the C1 s high resolution spectrum (Fig. S5), carbon was exclusively in graphitic form. In the high resolution spectrum of oxygen (Fig. S5) both carbon- and phosphorus-bonded atoms (or surface hydroxyls due to exposure to air) were seen as the O1 s signal, which was split into two components at 532.8 and 530.5 eV. Quantitative analyses (Fig. 3b) showed a phosphorus surface concentration of ~2.3 at.%, a relatively large content that resulted from effective chemical activation with phosphoric acid. Interestingly, phosphorus content did not change after functionalization and urea treatment, suggesting strong bonds within the carbon framework (Fig. 3b).

A small N1 s peak at ca. 400 eV (Fig. 3a) was evident in *AC-U-P* and *AC-F-U-P* samples, suggesting N-doping of the acti-
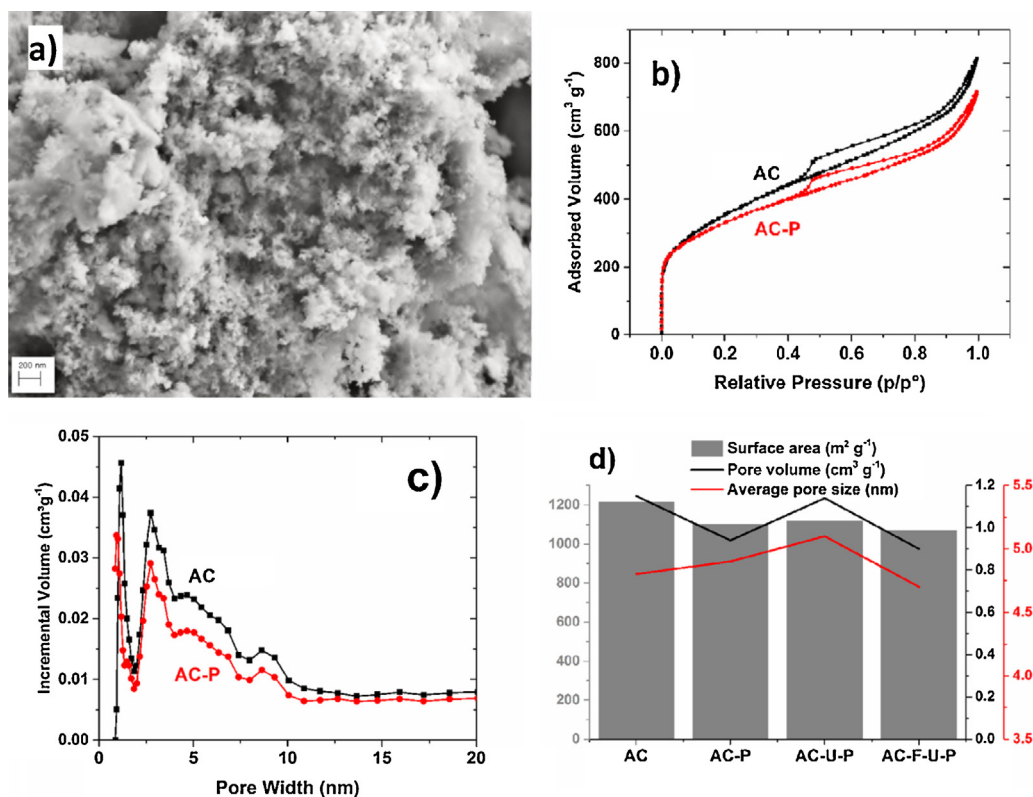
Fig. 2. SEM micrograph of activated carbon (*AC*) after chemical activation of ground coconut shells (a). N$_2$ adsorption isotherms of *AC* and *AC-P* (b). Pore distribution of *AC* and *AC-P* from DFT method (c).
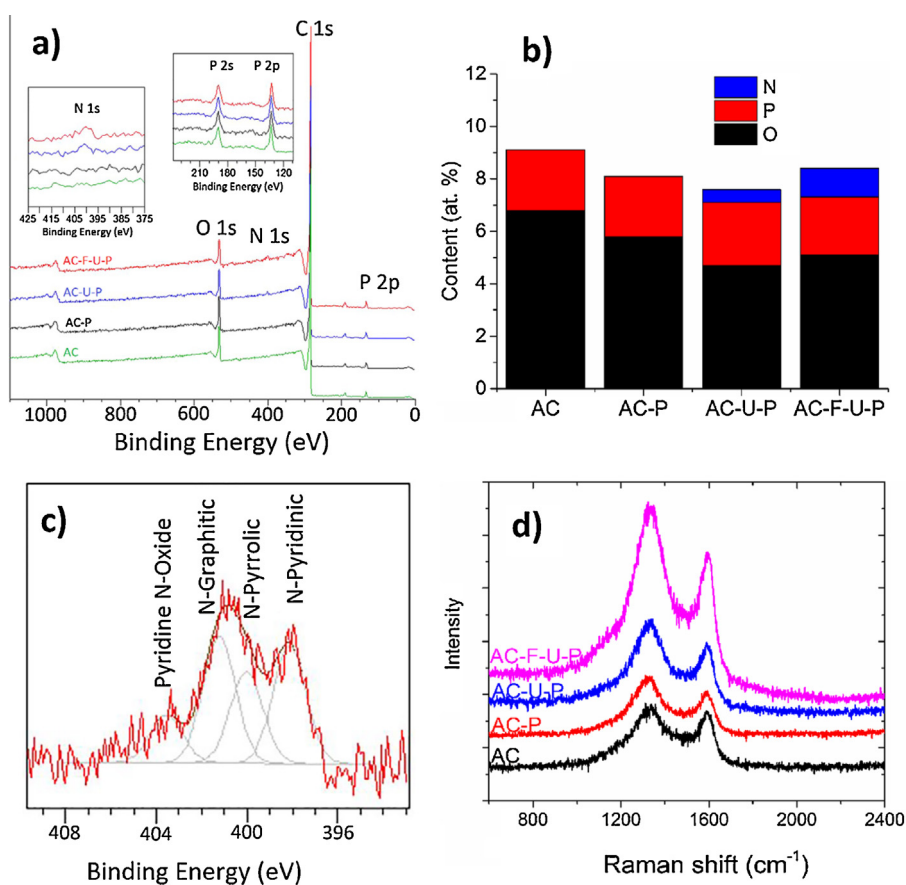

Fig. 3. XPS survey spectra of carbon samples (inset: high-resolution N*1 s* and P*2p* spectra) (a). Atomic% of elements present on the surface according to XPS (b). Deconvolution of high-resolution N*1 s* spectra with assigned N-functionalities (c) and Raman spectra of *AC, AC-P, AC-U-P, AC-F-U-P* samples (d).
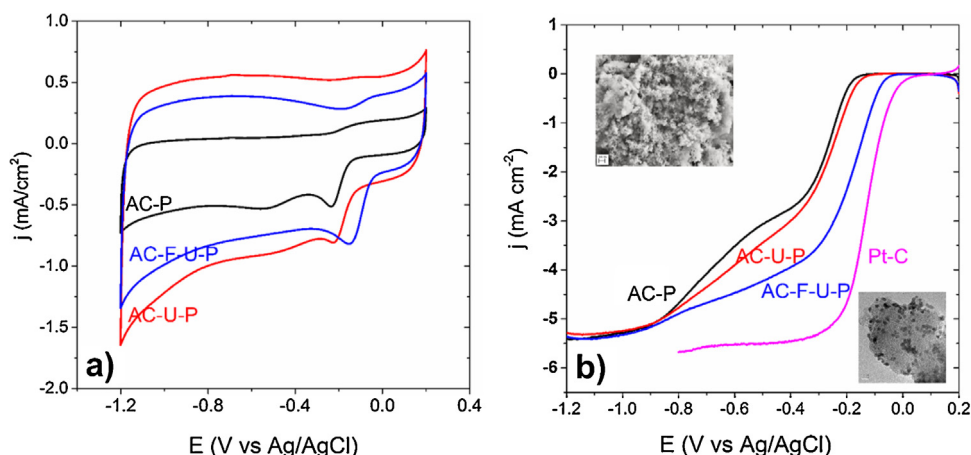
Fig. 4. Cyclic voltammograms recorded at 10 mV s^{-1} (a) and LSV at 1600 rpm in O$_2$-sturated 0.1 M KOH (b) of carbon samples derived from coconut shells, as indicated (the profile for commercial Pt-C is included for comparison).
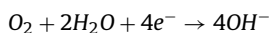
vated carbons after impregnation with urea. The nitrogen content almost doubled from 0.5 at.% (*AC-U-P*) to 1.1 at.% (*AC-F-U-P*), upon functionalization and enhanced interaction of urea with oxygen functional groups on the surface (Fig. 3b). A slight but measurable decrease in the O/C atomic ratio, from 0.06 (*AC-P*) to 0.05 (*AC-U-P*), was observed upon urea addition. The close relationship between the nitrogen doping and disappearance of oxygen-containing moieties suggest the occurrence of reactions of oxygen functional groups with the amine groups of urea [50]. This was also confirmed by FTIR spectra (Fig. S6). The deconvolution of N1 s peak of *AC-F-U-P* (Fig. 3c) showed the presence of four types of N-functionalities including N-pyridinic (398.4 eV, 31.1 at.%), N-pyrrolic (399.8 eV, 24.8 at.%), N-graphitic (401.5 eV, 33.6 at.%) and pyridine N-oxide (402.9 eV, 10.5 at.%). The high concentration of N-graphitic may be the result of the graphitic carbon nitride originated from urea and also the partial transformation of N-pyridinic into N-graphitic as the pyrolysis temperature increases to 1000 °C, due to the condensation of graphitic rings [52]. The N-pyridinic and N-graphitic have been recognized to impart high electrocatalytic activity for the ORR [53].

Raman spectra indicated the influence of N-doping treatments on the carbon structure (Fig. 3d). The D-band, the characteristic breathing mode of aromatic rings, occurred at 1340 cm^{-1}. The G-band, around 1590 cm^{-1}, assigned to the tangential vibration mode of carbon atoms. A high I_D/I_G ratio is typically indicative of more disordered carbon structures [54,55]. In the present case, the I_D/I_G values for *AC* and *AC-P* were similar, ~1.1; however, it increased to 1.25 for *AC-U-P*. It is well-known that the addition of heteroatoms in the graphitic carbon lattice structure results in more defects and a larger D-band intensity [56]. As expected further functionalization in *AC-F-U-P* created more defects, and resulted in an increased I_D/I_G value (~1.4).
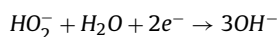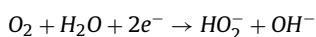
3.2. Electrochemical activity

The oxygen reduction reaction (ORR) in aqueous solutions mainly occurs through direct 4-electron reduction from O$_2$ to H$_2$O (OH$^-$ in alkaline) and the 2-electron reduction to H$_2$O$_2$ (HO$^-_2$ in alkaline) [57]:

4-electron process:

$$O_2 + 2H_2O + 4e^- \rightarrow 4OH^-$$

2-electron process:

$$O_2 + H_2O + 2e^- \rightarrow HO_2^- + OH^-$$

$$HO_2^- + H_2O + 2e^- \rightarrow 3OH^-$$

The electrocatalytic activity of the catalysts toward the ORR was first evaluated by cyclic voltammetry (CV) (Fig. 4a). Cyclic voltammograms of *AC-P* in O$_2$-sturated 0.1 M KOH clearly showed characteristic two step 2-electron reduction process, with peak potentials occurring at −0.23 and −0.6 V. In the case of *AC-U-P* electrode, the treatment with urea slightly improved the ORR activity (Fig. 4a). However, functionalization of the active carbon before pyrolysis enhanced the catalytic activity of *AC-F-U-P* by shifting the ORR peak potential to a more positive value (-0.15 V). Linear scan voltammograms (LSV) were recorded from the RDE measurements for each catalyst (Fig. 4b). The baseline currents were recorded in the absence of oxygen and subtracted from the polarization curves recorded in the O$_2$-saturated electrolyte, allowing determination of the onset potential for ORR. A shift of the onset potential towards more positive potentials, from −0.17 V (AC-P) to −0.15 V (AC-U-P) was observed. This transition further improved to −0.02 V for *AC-F-U-P*, much closer to the commercial Pt-C onset potential (0.05 V).

In order to quantify the kinetics of the ORR, the Koutecky-Levich (K-L) plots were derived from the LSV profiles at different rotation rates. The LSV profiles of *AC-F-U-P* at different rotation rates and the corresponding K-L plots at different potentials are presented in Fig. 5. The K-L plots were linear and near parallel, indicating a first-order reaction kinetics toward the ORR, and a similar electron transfer number (n) at the different potentials. The value of n can be calculated from the K-L equation [58]:

$$\frac{1}{j} = \frac{1}{j_k} + \frac{1}{j_d} = \frac{1}{j_k} + \frac{1}{0.6nFD_{O_2}^{2/3}\nu^{-1/6}C_{O_2}^b \omega^{1/2}}$$

where j is the overall current density, and j_k and j_d are the kinetic and diffusion-limited current densities, respectively. ω is the electrode rotation rate (rad s^{-1}), F is the Faraday constant (96486.4 C mol^{-1}); C_{O2} is the concentration of O$_2$ in 0.1 M KOH (1.26 × 10^{-6} mol cm^{-3}); D_{O2} is the diffusion coefficient of O$_2$ in 0.1 M KOH (1.9 × 10^{-5} cm^2 s^{-1}); ν is the kinematic viscosity of the electrolyte (0.01 cm^2 s^{-1}) [57].

The K-L plots for *AC* and *AC-P* (measured at −0.4 V) are presented for comparison in Fig. 5c, together with that of *AC-F-U-P*. The n value for all the samples was calculated from the slope of the K-L curves at the different potentials, and compared with that for the commercial Pt-C electrode (Fig. 5d). The average number of transferred electrons in the potential range between −0.3 and −0.5 V showed a significant improvement upon urea treatment, from n = 2.7 (*AC-P*) to 3.2 (*AC-U-P*), a remarkable change only with 0.5 at.% of nitrogen
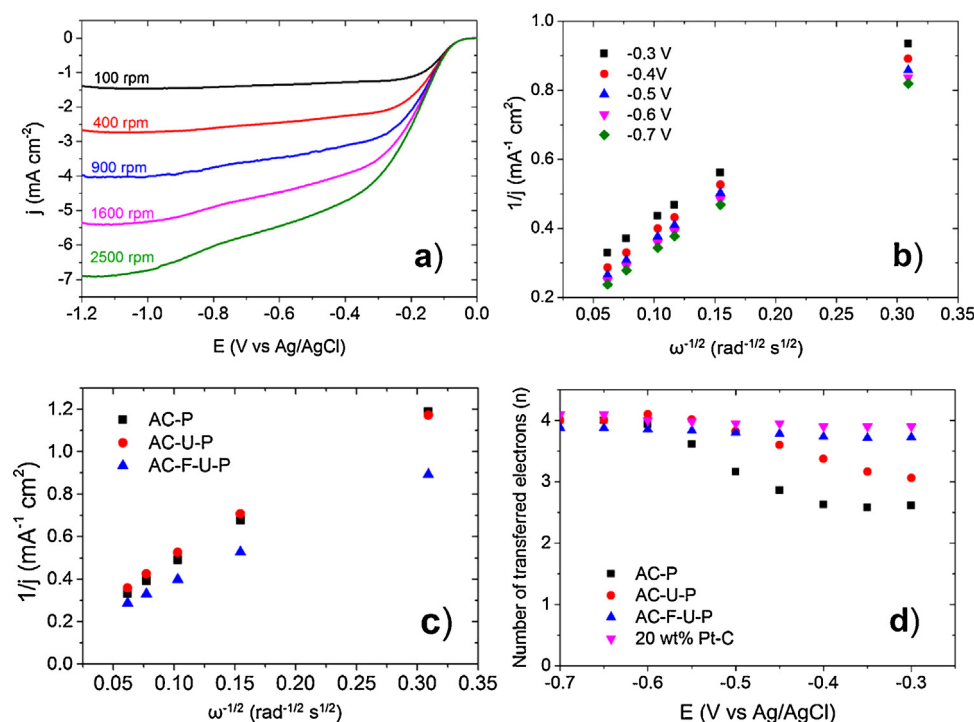
Fig. 5. LSV curves for the AC-F-U-P sample at different rotation rates in O_2-saturated 0.1 M KOH (a), K-L plots derived from (a) at different potentials (b), K-L plots at −0.4 V for *AC*, *AC-P* and *AC-F-U-P* derived from the respective LSV curves (c), and the electron transfer number calculated from the K-L equation at different potentials (d).
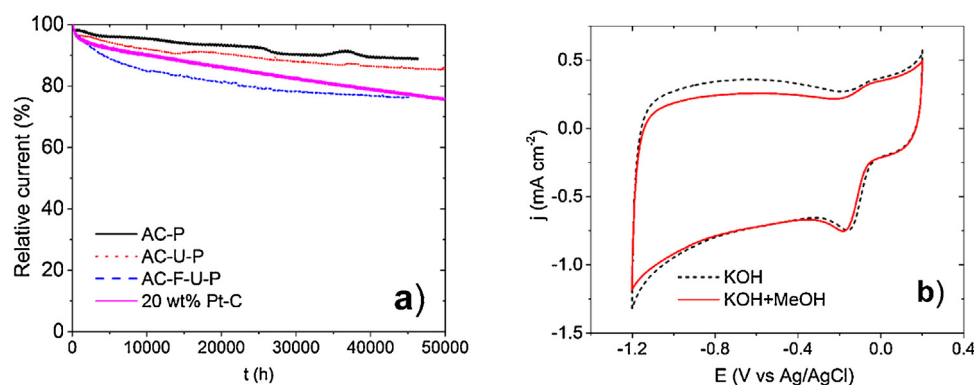

Fig. 6. Stability measurement by chronoamperometry at −0.3 V at 900 rpm for 13 h (a), methanol oxidation assessment for *AC-F-U-P* electrode with and without the presence of methanol (3 M) in O_2-saturated 0.1 M KOH.

doping. The value of *n* was further enhanced to ∼3.7 for *AC-F-U-P*, after functionalization was performed on the activated carbon.

It can be concluded that the functionalization treatment significantly affected the ORR electrocatalytic activity by providing more oxygen-containing functional groups on the surface of the activated carbon, which interact with urea and, consequently, increases the N-doping level. This observation has been also reported earlier for few-walled carbon nanotubes (FWCNTs) with polyaniline (PANI) used as nitrogen precursor, leading to a significantly enhanced ORR activity upon functionalization of pristine FWCNTs before doping with PANI [53].

The better ORR electrocatalytic activity observed at *AC-F-U-P* for ORR can be explained by the higher N content (1.1 at.%) in this sample. The exact role of nitrogen and its influence on the reduction of oxygen is still a controversial subject. In some cases, a direct correlation between N-doping level and an improved ORR activity has been observed [59,60]; in contrast, others have found no relation between the higher total nitrogen content and the ORR activity [61,59]. For example, a high ORR electrocatalytic activity

($n = 3.7$) was observed with very low nitrogen doping levels (0.5 at.%) in N-doped FWCNTs [53,62]. While in another study, N-CNTs containing nitrogen as high as 20 at.% provided much lower ORR catalytic activity (*n*: 2.6) [63]. The ORR activity of the *AC-F-U-P* system obtained from coconut shells in this study is compared with values from the literature corresponding to N-doped carbons from different biomass sources (Table 1).

The excellent electrocatalytic performance of the activated carbon obtained from coconut shells can also be ascribed to the high surface area and the large contribution of mesopores. Both factors enhance the mass transport of the liquid electrolyte. The governing influence of surface area on the catalytic activity (rather than the nitrogen content) was previously reported by Jaouen et al. [64]. The three-dimensional open pore structure provides enhanced accessibility of the oxygen molecules to the active sites [65], despite the low N content, together with the synergistic effect of P-heteroatom in the structure as reported earlier. We note that according to our previous findings, in the porous N-doped carbons with low nitrogen content, the adsorption of O_2 molecules likely occurs on N-graphitic

Table 1
Comparison results of the biomass-derived nitrogen-doped carbon materials. The ORR onset potential (E_{onset}) and half-wave potential ($E_{1/2}$) in O_2-saturated 0.1 M KOH are given with respect to Ag/AgCl.

Carbon precursor	Nitrogen precursor	Activating agent	Pyrolysis temp. (°C)	Surface area (m² g⁻¹)	Pore volume (cm³ g⁻¹)	Total N, P, S (at.%)	Electron transferred (n)	E_{onset} (V)	$E_{1/2}$ (V)	Refs.
Cellulose nanocrystals	Urea	–	1000	1362.36	3.36	3.51	–	–0.01	–0.13	[16]
Glucose/	Soy protein	–	1000	449	0.25	1.9	3.5	–0.07	–0.2	[17]
Cellulose microcrystalline				697	0.38	0.5	3.3	–0.15	–0.23	
Chitin	–	$ZnCl_2$	750	300.7	0.31	4.99	3.93	–0.2	–0.29	[19]
Chitosan	Urea	–	1000	1510	1.32	4.36	3.67	–0.03	–0.17	[22]
Eichhornia crassipes	–	$ZnCl_2$	700	950.6	1.49	4.76	3.51–3.82	0.02	–0.13	[24]
Typha orientalis	NH_3	–	800	898	0.52	9.1	3.7–4	–0.09	–0.24	[25]
Cellulose microcrystalline	$(NH_4)_3PO_4$	–	900		–	N:2.17 P:2.22	3.5	+0.2[a]	–0.31[a]	[27]
Human hair	–	NaOH	900	1813.65		N:3.8 S:1.7	3.8–3.9	–0.02	–0.14	[28]
Ginkgo leaves	NH_3	–	1000	1436.02	–	1.59	3.7	–0.04	–0.15	[31]
Seaweed	–	–	1000	1217.78	1.45	2.3	3.7	–0.01	–0.11	[32]
Coconut shells	Urea	H_3PO_4	1000	1071	0.9	N:1.1 P:2.3	3.7	–0.02	–0.21	This work

[a] Experiments were conducted in 50 mM phosphate buffer solution (pH = 7).

sites [5], followed by a fast decomposition or an electroreduction of hydroperoxide on N-pyridinic, overall leading to a fast conversion of oxygen molecules [65]. Taken together, the observations point to an ORR mechanism of the activated carbons involving an electron transfer number close to 4 (pseudo-4e⁻ mechanism), even at low nitrogen doping level. This is significant, mainly because the type of biomass used (inexpensive, widely available and in many cases considered a waste) and the simplicity of carbonization procedure.

3.3. Electrode stability and methanol tolerance

The long-term stability of the carbon samples was evaluated by chronoamperometry at −0.3 V (900 rpm for 50,000 s) (Fig. 6a). *AC-P* retained almost 90% of its initial activity after 13 h in continuous operation, which is quite significant. Treatment with urea (*AC-U-P*) only slightly degraded the durability to 85%. However, the functionalization that effectively increased the electroactivity (*AC-F-U-P* sample) undermined the electrode stability, reaching a plateau of about 75% after 13 h.

It is possible that the severe acid treatment performed on the activated carbon created more defects in the structure, as observed by Raman spectroscopy, leading to catalyst deactivation with time. However, we note that the decrease in current response can also be a consequence of detachment of the catalyst particles from the surface of the GCE, a highly probable factor given the high rotation speed during the 13 h-long test, as has been reported elsewhere [46]. Nevertheless, the durability of *AC-F-U-P* as measured by the performance after 13 h was close to that of the commercial Pt-C electrode. Furthermore, any possible degradation of *AC-F-U-P* seemed to slow down with time (plateau profile) while the degradation of Pt-C displayed a sharp slope to lower values. It is known that Pt-C deactivation occurs due to the susceptible oxidation or loss of Pt nanoparticles as well as the corrosion of the carbon black support. Overall, the stability of the developed nitrogen-doped electrocatalyst obtained from coconut shells is similar to the range of values reported for N-doped carbons from biomass, about 80–85% [25,28,31,46], but excels in the fact that the ORR activity is close to that measured for Pt-C used for benchmarking.

The tolerance of *AC-F-U-P* against methanol crossover was assessed in O_2-saturated 0.1 M KOH containing 3 M methanol (Fig. 6b). In the presence of methanol, the catalyst responded with the same peak current/position compared to the pure KOH electrolyte. This suggests excellent selectivity of *AC-F-U-P* toward the ORR, in contrast to Pt-C catalyst where a large current response was always observed (Fig. S7). Thus, as important advantage of the developed material is that it does not suffer from the major drawback observed in other systems with regards to the effect of methanol oxidation; i.e. the crossover issue in the case of Pt-C, that is methanol passing through the membrane, from the anode to the cathode compartment of the fuel cell, and methanol oxidation that competes for active sites as well as Pt-C catalyst CO poisoning [66].

4. Conclusions

Herein, a facile and cost-effective route for the valorization of residual biomass toward electroactive materials is demonstrated. Coconut shells were chosen due to the high lignin and low ash content in order to obtain higher product yield. Activated carbons were obtained in high yields (46%) by an optimized activation via phosphoric acid at mild temperatures (550 °C). The resulting carbon structures displayed high porosity (1260 m² g⁻¹ specific surface area, 1.15 cm³ g⁻¹ pore volume) and large mesopore volume (72%). Urea was used as a low-cost and ecologically-sound nitrogen source for improved electrocatalytic activity in ORR; it thus enabled N-doping of the activated carbon structure after pyrolysis. Despite a

relatively low nitrogen content, a high ORR activity was measured upon functionalization of the coconut-derived carbon, comparable to that of a reference commercial Pt-C catalyst. Moreover, the porous carbon catalysts showed excellent long-term stability and tolerance toward methanol oxidation. Such exceptional catalytic performance can be ascribed to the unique hierarchical porous structure of the obtained materials, which also benefit from (a) the contribution of a large fraction of mesopores that provides enhanced electrolyte mass transport and easy access of oxygen molecules to the active sites; (b) the synergic effect of N and P doping, and (c) large proportion of active nitrogen species (N-graphitic and N-pyridinic). The prepared material is not only promising alternative to Pt-containing electrocatalysts for alkaline fuel cells, but is also attractive for other applications such as supercapacitors, catalytic conversion, electrochemical sensors and gas sorbents.

Acknowledgments

Appendix A. Supplementary data

Supporting information available online includes TGA analysis of pristine coconut shells compared to that of coconut shells impregnated with phosphoric acid; N2 isotherms and pore distribution by DFT method for AC-U-P and AC-F-U-P; illustration of the influence of functionalization time on the active carbon pore structure; wide and high-resolution XPS spectra of the C1 s and O1s; FTIR spectra of activated carbon doped with urea before and after functionalization (AC, AC-U, AC-F and AC-F-U) and methanol oxidation assessment for commercial Pt-C catalyst with and without methanol (3 M) in O2-saturated 0.1 M KOH.

Supplementary data associated with this article can be found, in the online version, at http://dx.doi.org/10.1016/j.apcatb.2016.11.029.

References

[1] W.Y. Wong, W.R.W. Daud, A.B. Mohamad, A.A.H. Kadhum, E.H. Majlan, K.S. Loh, Nitrogen-containing carbon nanotubes as cathodic catalysts for proton exchange membrane fuel cells, Diam. Relat. Mater. 22 (2012) 12–22.

[2] X. Zhao, M. Yin, L. Ma, L. Liang, C. Liu, J. Liao, T. Lu, W. Xing, Recent advances in catalysts for direct methanol fuel cells, Energy Environ. Sci. 4 (2011) 2736–2753.

[3] F. Jaouen, E. Proietti, M. Lefèvre, R. Chenitz, J.-P. Dodelet, G. Wu, H.T. Chung, C.M. Johnston, P. Zelenay, Recent advances in non-precious metal catalysis for oxygen-reduction reaction in polymer electrolyte fuel cells, Energy Environ. Sci. 4 (2011) 114–130.

[4] D. Yu, E. Nagelli, F. Du, L. Dai, Metal-free carbon nanomaterials become more active than metal catalysts and last longer, J. Phys. Chem. Lett. 1 (2010) 2165–2173.

[5] D. Srivastava, T. Susi, M. Borghei, L. Kari, Dissociation of oxygen on pristine and nitrogen-doped carbon nanotubes: a spin-polarized density functional study, RSC Adv. 4 (2014) 15225–15235.

[6] P. Ayala, R. Arenal, M. Rümmeli, A. Rubio, T. Pichler, The doping of carbon nanotubes with nitrogen and their potential applications, Carbon N. Y. 48 (2010) 575–586.

[7] M. Terrones, A.G.S. Filho, A.M. Rao, Doped carbon nanotubes: synthesis, characterization and applications, in: Carbon Nanotuibes, Springer, 2008, pp. 531–566.

[8] S. Ni, Z.Y. Li, J.L. Yang, Oxygen molecule dissociation on carbon nanostructures with different types of nitrogen doping, Nanoscale 4 (2012) 1184–1189.

[9] V.V. Strelko, V.S. Kuts, P.A. Thrower, On the mechanism of possible influence of heteroatoms of nitrogen, boron and phosphorus in a carbon matrix on the catalytic activity of carbons in electron transfer reactions, Carbon 38 (2000) 1499–1524.

[10] D. Yu, Y. Xue, L. Dai, Vertically aligned carbon nanotube arrays co-doped with phosphorus and nitrogen as efficient metal-free electrocatalysts for oxygen reduction, J. Phys. Chem. Lett. 3 (2012) 2863–2870.

[11] K.A. Shah, B.A. Tali, Synthesis of carbon nanotubes by catalytic chemical vapour deposition: a review on carbon sources, catalysts and substrates, Mater. Sci. Semicond. Process. 41 (2016) 67–82.

[12] J. United Nations Environmental Programme Division of Technology, Industry and Economics International Environmental Technology Centre Osaka/Shiga, Converting Waste Agricultural Biomass into a Resource, United Nations Environ. Program, (2009) 1–437.

[13] S. De, A.M. Balu, J.C. Van Der Waal, R. Luque, Biomass-derived porous carbon materials: synthesis and catalytic applications, ChemCatChem 7 (2015) 1608–1629.

[14] C. Long, D. Qi, T. Wei, J. Yan, L. Jiang, Z. Fan, Nitrogen-doped carbon networks for high energy density supercapacitors derived from polyaniline coated bacterial cellulose, Adv. Funct. Mater. 24 (2014) 3953–3961.

[15] L.F. Chen, Z.H. Huang, H.W. Liang, H.L. Gao, S.H. Yu, Three-dimensional heteroatom-doped carbon nanofiber networks derived from bacterial cellulose for supercapacitors, Adv. Funct. Mater. 24 (2014) 5104–5111.

[16] Q. Liu, C. Chen, F. Pan, J. Zhang, Highly efficient oxygen reduction on porous nitrogen-doped nanocarbons directly synthesized from cellulose nanocrystals and urea, Electrochim. Acta 170 (2015) 234–241.

[17] S.-M. Alatalo, K. Qiu, K. Preuss, A. Marinovic, M. Sevilla, M. Sillanpää, X. Guo, M.-M. Titirici, Soy protein directed hydrothermal synthesis of porous carbon aerogels for electrocatalytic oxygen reduction, Carbon N. Y. 96 (2016) 622–630.

[18] T.-D. Nguyen, K.E. Shopsowitz, M.J. MacLachlan, Mesoporous nitrogen-doped carbon from nanocrystalline chitin assemblies, J. Mater. Chem. A 2 (2014) 5915–5921.

[19] H. Yuan, L. Deng, X. Cai, S. Zhou, Y. Chen, Y. Yuan, RSC Advances Nitrogen-doped carbon sheets derived from chitin as non-metal bifunctional electrocatalysts for oxygen reduction and evolution †, RSC Adv. 5 (2015) 56121–56129.

[20] A. Primo, P. Atienzar, E. Sanchez, J.M. Delgado, H. García, From biomass wastes to large-area, high-quality, N-doped graphene: catalyst-free carbonization of chitosan coatings on arbitrary substrates, Chem. Commun. 48 (2012) 9254.

[21] M.K. Rybarczyk, M. Lieder, M. Jablonska, N-doped mesoporous carbon nanosheets obtained by pyrolysis of a chitosan-melamine mixture for the oxygen reduction reaction in alkaline media, RSC Adv. 5 (2015) 44969–44977.

[22] Q. Liu, Y. Duan, Q. Zhao, F. Pan, B. Zhang, J. Zhang, Direct synthesis of nitrogen-doped carbon nanosheets with high surface area and excellent oxygen reduction performance, Langmuir 30 (2014) 8238–8245.

[23] Y. Yang, Y. Deng, Z. Tong, C. Wang, Renewable lignin-based xerogels with self-cleaning properties and superhydrophobicity, ACS Sustain. Chem. Eng. 2 (2014) 1729–1733.

[24] X. Liu, Y. Zhou, W. Zhou, L. Li, S. Huang, S. Chen, Biomass-derived nitrogen self-doped porous carbon as effective metal-free catalysts for oxygen reduction reaction, Nanoscale 7 (2015) 6136–6142.

[25] P. Chen, L.-K. Wang, G. Wang, M.-R. Gao, J. Ge, W.-J. Yuan, Y.-H. Shen, A.-J. Xie, S.-H. Yu, Nitrogen-doped nanoporous carbon nanosheets derived from plant biomass: an efficient catalyst for oxygen reduction reaction, Energy Environ. Sci. 7 (2014) 4095–4103.

[26] Q. Liu, S. Chen, Y. Zhou, S. Zheng, H. Hou, F. Zhao, Phosphorus-doped carbon derived from cellulose phosphate as efficient catalyst for air-cathode in microbial fuel cells, J. Power Sour. 261 (2014) 245–248.

[27] Q. Liu, Y. Zhou, S. Chen, Z. Wang, H. Hou, F. Zhao, Cellulose-derived nitrogen and phosphorus dual-doped carbon as high performance oxygen reduction catalyst in microbial fuel cell, J. Power Sour. 273 (2015) 1189–1193.

[28] K.N. Chaudhari, M.Y. Song, J.S. Yu, Transforming hair into heteroatom-doped carbon with high surface area, Small 10 (2014) 2625–2636.

[29] S.-A. Wohlgemuth, R.J. White, M.-G. Willinger, M.-M. Titirici, M. Antonietti, A one-pot hydrothermal synthesis of sulfur and nitrogen doped carbon aerogels with enhanced electrocatalytic activity in the oxygen reduction reaction, Green Chem. 14 (2012) 1515–1523.

[30] L. Roldan, Y. Marco, E. Garcia-Bordeje, Bio-sourced mesoporous carbon doped with heteroatoms (N,S) synthesised using one-step hydrothermal process for water remediation, Microporous Mesoporous Mater. 222 (2016) 55–62.

[31] F. Pan, Z. Cao, Q. Zhao, H. Liang, J. Zhang, Nitrogen-doped porous carbon nanosheets made from biomass as highly active electrocatalyst for oxygen reduction reaction, J. Power Sour. 272 (2014) 8–15.

[32] M.Y. Song, H.Y. Park, D.S. Yang, D. Bhattacharjya, J.S. Yu, Seaweed-derived heteroatom-doped highly porous carbon as an electrocatalyst for the oxygen reduction reaction, ChemSusChem 7 (2014) 1755–1763.

[33] K. Yang, J. Peng, C. Srinivasakannan, L. Zhang, H. Xia, X. Duan, Preparation of high surface area activated carbon from coconut shells using microwave heating, Bioresour. Technol. 101 (2010) 6163–6169.

[34] W. Li, K. Yang, J. Peng, L. Zhang, S. Guo, H. Xia, Effects of carbonization temperatures on characteristics of porosity in coconut shell chars and activated carbons derived from carbonized coconut shell chars, Ind. Crops Prod. 28 (2008) 190–198.

[35] M.J. Prauchner, F. Rodríguez-Reinoso, Chemical versus physical activation of coconut shell: a comparative study, Microporous Mesoporous Mater. 152 (2012) 163–171.

[36] T. Rout, D. Pradhan, R.K. Singh, N. Kumari, Exhaustive study of products obtained from coconut shell pyrolysis, J. Environ. Chem. Eng. 4 (2016) 3696–3705.

[37] W. Heschel, E. Klose, On the suitability of agricultural by-products for the manufacture of granular activated carbon, Fuel 74 (1995) 1786–1791.

[38] M. Yang, L. Guo, G. Hu, X. Hu, L. Xu, J. Chen, W. Dai, M. Fan, Highly cost-effective nitrogen-doped porous coconut shell-based CO2 sorbent synthesized by combining ammoxidation with KOH activation, Environ. Sci. Technol. 49 (2015) 7063–7070.

[39] W. Zhao, M. Sun, H. Zhang, Y. Dong, X. Li, W. Li, J. Zhang, Catalytic dehydrochlorination of 1,2-dichloroethane to produce vinyl chloride over N-doped coconut activated carbon, RSC Adv. 5 (2015) 104071–104078.

[40] J. Mi, X.-R. Wang, R.-J. Fan, W.-H. Qu, W.-C. Li, Coconut-shell-based porous carbons with a tunable micro/mesopore ratio for high-performance supercapacitors, Energy Fuels 26 (2012) 5321–5329.

[41] A. Jain, S.K. Tripathi, Fabrication and characterization of energy storing supercapacitor devices using coconut shell based activated charcoal electrode, Mater. Sci. Eng. B 183 (2014) 54–60.

[42] R.G. Pereira, C.M. Veloso, N.M. da Silva, L.F. de Sousa, R.C.F. Bonomo, A.O. de Souza, M.O. da G. Souza, R. da C.I. Fontan, Preparation of activated carbons from cocoa shells and siriguela seeds using H3PO4 and ZnCL2 as activating agents for BSA and α-lactalbumin adsorption, Fuel Process. Technol. 126 (2014) 476–486.

[43] W.C. Lim, C. Srinivasakannan, N. Balasubramanian, Activation of palm shells by phosphoric acid impregnation for high yielding activated carbon, J. Anal. Appl. Pyrolysis. 88 (2010) 181–186.

[44] X. Wang, D. Li, W. Li, J. Peng, H. Xia, L. Zhang, S. Guo, G. Chen, Optimization of mesoporous activated carbon from coconut shells by chemical activation with phosphoric acid, BioResources 8 (2013) 6184–6195.

[45] G. Dong, Y. Zhang, Q. Pan, J. Qiu, A fantastic graphitic carbon nitride (g-C3N4) material: electronic structure, photocatalytic and photoelectronic properties, J. Photochem. Photobiol. C Photochem. Rev. 20 (2014) 33–50.

[46] Q. Liu, Y. Duan, Q. Zhao, F. Pan, B. Zhang, J. Zhang, Direct synthesis of nitrogen-doped carbon nanosheets with high surface area and excellent oxygen reduction performance, Langmuir 30 (2014) 8238–8245.

[47] T. Khadiran, M.Z. Hussein, Z. Zainal, R. Rusli, Textural and chemical properties of activated carbon prepared from tropical peat soil by chemical activation method, Bioresources 10 (2015) 986–1007.

[48] S. Ouyang, S. Xu, N. Song, S. Jiao, Coconut shell-based carbon adsorbents for ventilation air methane enrichment, Fuel 113 (2014) 420–425.

[49] M. Jagtoyen, F. Derbyshire, Activated carbons from yellow poplar and white oak by H3PO4 activation, Carbon N. Y. 36 (1998) 1085–1097.

[50] Z.-H. Sheng, L. Shao, J.-J. Chen, W.-J. Bao, F.-B. Wang, X.-H. Xia, Catalyst-free synthesis of nitrogen- doped graphene via thermal annealing graphite oxide with melamine and its excellent electrocatalysis, ACS Nano 5 (2011) 4350–4358.

[51] L. Li, S. Liu, J. Liu, Surface modification of coconut shell based activated carbon for the improvement of hydrophobic VOC removal, J. Hazard. Mater. 192 (2011) 683–690.

[52] T. Sharifi, G. Hu, X. Jia, T. Wagberg, Formation of active sites for oxygen reduction reactions by transformation of nitrogen functionalities in nitrogen-doped carbon nanotubes, ACS Nano 6 (2012) 8904–8912.

[53] M. Borghei, P. Kanninen, M. Lundahl, T. Susi, J. Sainio, I. Anoshkin, A. Nasibulin, T. Kallio, K. Tammeveski, E. Kauppinen, V. Ruiz, High oxygen reduction activity of few-walled carbon nanotubes with low nitrogen content, Appl. Catal. B Environ. 158–159 (2014) 233–241.

[54] M.S. Dresselhaus, G. Dresselhaus, R. Saito, A. Jorio, Raman spectroscopy of carbon nanotubes, Phys. Rep. 409 (2005) 47–99.

[55] S. Kundu, W. Xia, W. Busse, M. Becker, D. Schmidth, A.M. Havenith, M. Muhler, The formation of nitrogen-containing functional groups on carbon nanotube surfaces: a quantitative XPS and TPD study, Phys. Chem. Chem. Phys. 12 (2010) 4351–4359.

[56] T. Sharifi, F. Nitze, H.R. Barzegar, C.W. Tai, M. Mazurkiewicz, A. Malolepszy, L. Stobinski, T. W??gberg, Nitrogen doped multi walled carbon nanotubes produced by CVD-correlating XPS and Raman spectroscopy for the study of nitrogen inclusion, Carbon N. Y. 50 (2012) 3535–3541.

[57] C. Song, J. Zhang, Electrocatalytic oxygen reduction reaction, PEM Fuel Cell Electrocatal. Catal. Layers Fundam. Appl. (2008) 89–134.

[58] M. Vikkisk, I. Kruusenberg, U. Joost, E. Shulga, I. Kink, K. Tammeveski, Electrocatalytic oxygen reduction on nitrogen-doped graphene in alkaline media, Appl. Catal. B Environ. 147 (2014) 369–376.

[59] T.C. Nagaiah, S. Kundu, M. Bron, M. Muhler, W. Schuhmann, Nitrogen-doped carbon nanotubes as a cathode catalyst for the oxygen reduction reaction in alkaline medium, Electrochem. Comm. 12 (2010) 338–341.

[60] Z. Chen, D. Higgins, Z. Chen, Nitrogen doped carbon nanotubes and their impact on the oxygen reduction reaction in fuel cells, Carbon N. Y. 48 (2010) 3057–3065.

[61] H.-S. Oh, J.-G. Oh, W.H. Lee, H.-J. Kim, H. Kim, The influence of the structural properties of carbon on the oxygen reduction reaction of nitrogen modified carbon based catalysts, Int. J. Hydrogen Energy 36 (2011) 8181–8186.

[62] P. Kanninen, M. Borghei, O. Sorsa, E. Pohjalainen, E.I. Kauppinen, V. Ruiz, T. Kallio, Highly efficient cathode catalyst layer based on nitrogen-doped carbon nanotubes for the alkaline direct methanol fuel cell, Appl. Catal. B Environ. 156–157 (2014) 341–349.

[63] Z. Wang, R. Jia, J. Zheng, J. Zhao, L. Li, J. Song, Z. Zhu, Nitrogen-promoted self-assembly of N-doped carbon nanotubes and their intrinsic catalysis for oxygen reduction in fuel cells, ACS Nano 5 (2011) 1677–1684.

[64] F. Jaouen, M. Lefevre, J.-P. Dodelet, M. Cai, Heat-treated Fe/N/C catalysts for O2 electroreduction: are active sites hosted in micropores? J. Phys. Chem. B 110 (2006) 5553–5558.

[65] M. Borghei, Novel Carbon Nanomaterials for the Direct Methanol Fuel Cell Electrodes, Aalto University publication series, 2015.

[66] I. Kruusenberg, S. Ratso, M. Vikkisk, P. Kanninen, T. Kallio, A.M. Kannan, K. Tammeveski, Highly active nitrogen-doped nanocarbon electrocatalysts for alkaline direct methanol fuel cell, J. Power Sour. 281 (2015) 94–102.